## Erratum

# Editorial Expression of Concern: Ballistic superconductivity in semiconductor nanowires (Nature communications)

Zhang, Hao; Gül, Önder; Conesa-Boj, Sonia; Nowak, Michał P.; Wimmer, Michael; de Vries, Folkert K.; van Veen, Jasper; de Moor, Michiel W.A.; Bommer, Jouri D.S.; van Woerkom, David J.

**DOI**
10.1038/s41467-025-58136-3

**Publication date**
2025

**Document Version**
Final published version

**Published in**
Nature Communications

# Editorial Expression of Concern: Ballistic superconductivity in semiconductor nanowires

Editorial Expression of Concern to:
*Nature Communications*
https://doi.org/10.1038/ncomms16025,
published online 06 July 2017

https://doi.org/10.1038/s41467-025-58136-3

Published online: 03 April 2025

Check for updates

Hao Zhang, Önder Gül, Sonia Conesa-Boj, Michał P. Nowak, Michael Wimmer, Folkert K. de Vries, Jasper van Veen, Michiel W. A. de Moor, Jouri D. S. Bommer, David J. van Woerkom, Diana Car, Sébastien R. Plissard, Erik P. A. M. Bakkers, Marina Quintero-Pérez, Maja C. Cassidy, Sebastian Koelling, Srijit Goswami, Kenji Watanabe, Takashi Taniguchi & Leo P. Kouwenhoven

*Nature Communications* is publishing an editorial expression of concern on the article "Ballistic superconductivity in semiconductor nanowires", by H. Zhang et al.

On 09 December 2021, the Editorial Staff was alerted by Vincent Mourik and two other researchers to potential problems in the manner in which raw data have been selected, processed and analysed. In response to these concerns, *Nature Communications* initiated an investigation by contacting the corresponding authors of the article and consulting with two independent experts. The investigation involved technical scrutiny of the additional analyses provided by the corresponding authors, including supplementary data from the repository https://zenodo.org/records/6851435. Based on the evidence presented, the Reviewers endorsed the publication of the correction note appended below.

Readers are urged to take this information into consideration when interpreting the data presented in this article.

Kun Zuo and Vincent Mourik also informed the editorial staff that they wished to be removed from authorship because in their opinion, the correction does not address the concerns with respect to the data and they do not endorse the validity of the claims and conclusions of the article. The author list in both the PDF and HTML has now been rectified.

All authors, with the exception of Kenji Watanabe and Takashi Taniguchi, disagree with the publication of this Editorial Expression of Concern.

**Correction note**

The Article reports structural analyses and transport measurements of hybrid InSb semiconductor nanowire–NbTiN superconductor devices. The devices exhibit a conductance plateau near the conductance quantum $2e^2/h$ at bias voltages above the superconducting gap (normal conductance), accompanied by an enhanced Andreev conductance at bias voltages below the superconducting gap (subgap conductance). We have attributed these experimental observations to ballistic transport supported by a theoretical analysis finding mean free paths in the order of or larger than the effective wire segment (the segment covered by the superconducting electrode).

Here, we correct errors discovered upon reanalysis of the original data[1] and provide an extended discussion to the claim of ballistic transport as to avoid misinterpretations. The claims in the Article remain.

Note that the original processing of the experimental data was done by H. Zhang and Ö. Gül, and the theoretical simulations were originally performed by M. P. Nowak and M. Wimmer, as stated in the original author contributions. The data processing of this correction note was done by Ö. Gül and M. Wimmer.

**Extended discussion**

1. Ballistic transport implies that all transmission eigenchannels that contribute to transport are close to 1. An extended transmission eigenchannel analysis[1] shows that all five devices reported in the Article exhibit a single transmission eigenchannel rising to nearly 1 and staying near this value while other eigenchannels stay close to 0 before also rising to larger values (New S. Figure 7 and 8). This behaviour is expected for a quantum point contact. The physical system of a quantum point contact can continuously evolve to a strongly coupled, broad resonance, for example when there is weak scattering and Fabry-Perot-like

resonances appear. Our experiments do not allow for discriminating between such scenarios. However, a broad resonance giving rise to an isolated transmission eigenchannel with near unit transmission also exhibits ballistic transport over a finite energy window, a scenario for which the claims in the Article remain also valid.

2. Our earlier studies on ballistic transport in nanowire devices[2,3] indicate that vapour-liquid-solid nanowires do not have the proper geometry for observing a conductance staircase (multiple plateaus) without the application of a magnetic field perpendicular to the wire axis. A conductance staircase without perpendicular field requires ideal (Landauer) reservoirs interfacing to the ballistic region, absorbing charge carriers with near-unit probability. Similar to our earlier studies, ohmic (normal metal) contacts in the present nanowire devices do not satisfy the conditions of Landauer reservoirs. However, the transport in the effective wire segment can nevertheless be ballistic whose characteristic is a plateau feature near $2e^2/h$ in normal conductance together with an enhanced Andreev conductance. In summary, a plateau feature with an enhanced Andreev conductance together with our theoretical analyses indicate that a large fraction of transport is ballistic over the distance between the superconducting and the normal metal contact, the definition of ballistic used in the Article.
3. The claims in the Article do not rely on the presented numerical calculations. The calculations only serve as additional corroboration. The main theoretical finding is that even for a nearly perfect QPC, very weak scattering leads to a reduction of the Andreev enhancement near the opening of additional QPC channels, qualitatively explaining the conductance dip prevalent in our experiments as well as in other works[4,5]. This combined enhancement-dip feature is used to estimate a mean free path in the experiment. (We note that such an estimate needs to be taken with the appropriate caution as a numerical simulation can never be a faithful representation of a real device).

   As stated in Methods, Details of the theoretical simulation, the mean free path in the calculations is related to the disorder which is represented as random on-site potential, a common model in transport calculations. The disorder induces mode mixing and results in the reduction of the conductance of the otherwise clean nanowire from $G = e^2/h \cdot N$ to $\langle G \rangle = e^2/h \cdot N/(1 + 3L/4l_e)$, where N is the number of transverse modes, L the length of the wire, and $l_e$ the elastic mean free path[6]. The strength of the random onsite disorder $U_0$ can be analytically related to the elastic mean free path through Fermi's golden rule, giving rise to the expression stated in Methods, Details of the theoretical simulation.

**Correction of technical errors**

A. In the dataset presented in Figure 3c (same as S. Figure 4b), and S. Figure 1i, n, a charge jump was corrected by removal of ten traces (corresponding to −1.34 … −1.25 V in gate voltage) where the gate voltage axis before the charge jump (−2.5 … −1.35 V) was offset by 0.1 V to maintain the continuity of the axis. This processing was regrettably not mentioned in the publication. Corrected Figure 3c and S. Figure 1i excludes this processing and represents the data as measured.
B. In the same dataset we have noticed that
   I. There was no exclusion of 0.5 kΩ (on-chip contact+lead resistance of the normal metal electrode), contrary to what was stated in the manuscript (As stated in Methods—'In all our analysis, we only subtract a fixed-value series resistance of 0.5 kΩ solely to account for the contact resistance of the normal metal lead.'). This error concerns Figure 3c (same as S. Figure 4b), and S. Figure 1i, n.
   II. In Figure 3c (same as S. Figure 4b), bias voltage was determined using an incorrect value for the external resistances which are fridge lines, fridge filters, and input and output impedances of the voltage source and current amplifiers. For the fridge in which this device was measured, these total to 8.1 kΩ. Instead, the bias axis was determined using the value of 7.28 kΩ corresponding to a different fridge. (Plotted conductance, however, was determined correctly using an accurate value for the external resistances.)
   III. In Figure 3c (same as S. Figure 4b), the bias voltage value above which the above-gap conductance $G_n$ was extracted from (0.8 mV) is not sufficiently large compared to the superconducting gap (the required condition for $G_n$). As a result, the plotted $G_n$ exceeds the conductance quantum $2e^2/h$ by ~1%.

      Corrected Figure 3c shows that the $G_n$ plotted in the paper minimally deviates from the corrected one which uses 8.1 kOhm for the external resistances and excludes 0.5 kOhm to account for the contact resistance of the normal metal lead. Subgap conductance $G_s$ after corrections is larger than the $G_s$ plotted in the paper indicating that the actual interface transparency is in fact *higher* than that reported in the paper (Corrected Figure 3c). As such, this error has no consequence on the claims of the paper.
C. In inset to Figure 4d, $G_n$ values (above-gap conductance as a function of gate voltage) and $G_s$ values (subgap conductance as a function of gate voltage, measured at different magnetic fields B) are taken from separate measurements at different times. This is because the four measurements the $G_s$ values are taken from excluded the large bias voltages from which $G_n$ can be determined. ($G_s$ measurements cover a bias voltage range $|V| < \sim 0.9$ mV over the entire gate voltage range whereas $G_n$ was determined from 1.5 mV < |V| < 2 mV.) For clarity, we denote the measurement from which the $G_n$ values are derived as $G_1^{B=0T}$, and the measurements from which $G_s$ values are derived as $G_2^{B=0T}$, $G_2^{B=0.25T}$, $G_2^{B=0.5T}$, $G_2^{B=0.75T}$.
   I. The gate voltage axis of $G_1^{B=0T}$ was offset by 1.62 V to compensate for an apparent shift in gate voltage between $G_1^{B=0T}$ and the four $G_2^{B=0\ldots0.75T}$. (Such shifts between measurements generally originate from a charge jump occurring in between.) This processing was regrettably not mentioned in the publication. New S. Figure 9 shows $G_1^{B=0T}$ and $G_2^{B=0T}$ without an offset, representing the data as measured. $G_1^{B=0T}$ and $G_2^{B=0T}$ are virtually identical justifying this processing.
   II. $G_s$ values at finite B are plotted against Gn values measured at zero field, regrettably not mentioned in the publication. New S. Figure 10 shows conductance traces from $Gs^{B=0T}$, $Gs^{B=0.25T}$, $Gs^{B=0.5T}$, $Gs^{B=0.75T}$ taken at V = 1.1 mV. All four traces are virtually identical, indicating that increasing B does not significantly affect conductances above the gap, which justifies this processing.

Additionally, the behaviour shown in the inset of Figure 4d is also reproduced in devices B and C, where Gs vs Gn plot can be directly extracted from the data excluding the processing steps above, shown in our new extended analysis[1].

D. In several figures, conductance (as a function of gate voltage) has been averaged over a bias voltage window, regrettably not mentioned in the publication, which smoothens the traces by removing the fast fluctuations.

| | $G_n$ | $G_s$ |
|---|---|---|
| Figure 2d | 1.85 mV < \|V\| < 2 mV | \|V\| < 150 μV |
| Figure 2e (same as S. Figure 4a) | −1.55 mV < V < −1.45 mV | \|V\| < 50 μV |
| Figure 3c (same as S. Figure 4b) | 0.8 mV < V < 1 mV | \|V\| < 20 μV |
| Figure 4a | 1.7 mV < \|V\| < 1.96 mV | \|V\| < 190 μV |
| Figure 4d | 1.5 mV < \|V\| < 2 mV | *no averaging* |
| Figure 4d inset | *same data as Figure 4d* | *no averaging* |

New S. Figure 11 shows the originally published traces along with unaveraged ones, indicating minimal deviation between them. (See also Corrected Figure 3c where $G_n$ and $G_s$ are plotted for V = 1 mV and 0 mV without averaging.) Our new extended analysis[1], shown in New S. Figure 7 and 8, finds that all these differently obtained conductance traces (averaged bias |V|; positive bias V > 0; and negative bias V < 0) lead to the same conclusion: near-unit transmission of a single mode at the conductance plateau. As such, this processing does not affect the claims in any way.

E. In Methods, Details of the theoretical simulation, the equation for the amplitude $U_0$ uses atomic units convention which was not explicitly mentioned. In SI units, the equation reads $U_0 = \hbar^2\sqrt{3\pi/l_e m^{*2} a^3}$ (with the addition of a factor $\hbar^2$).

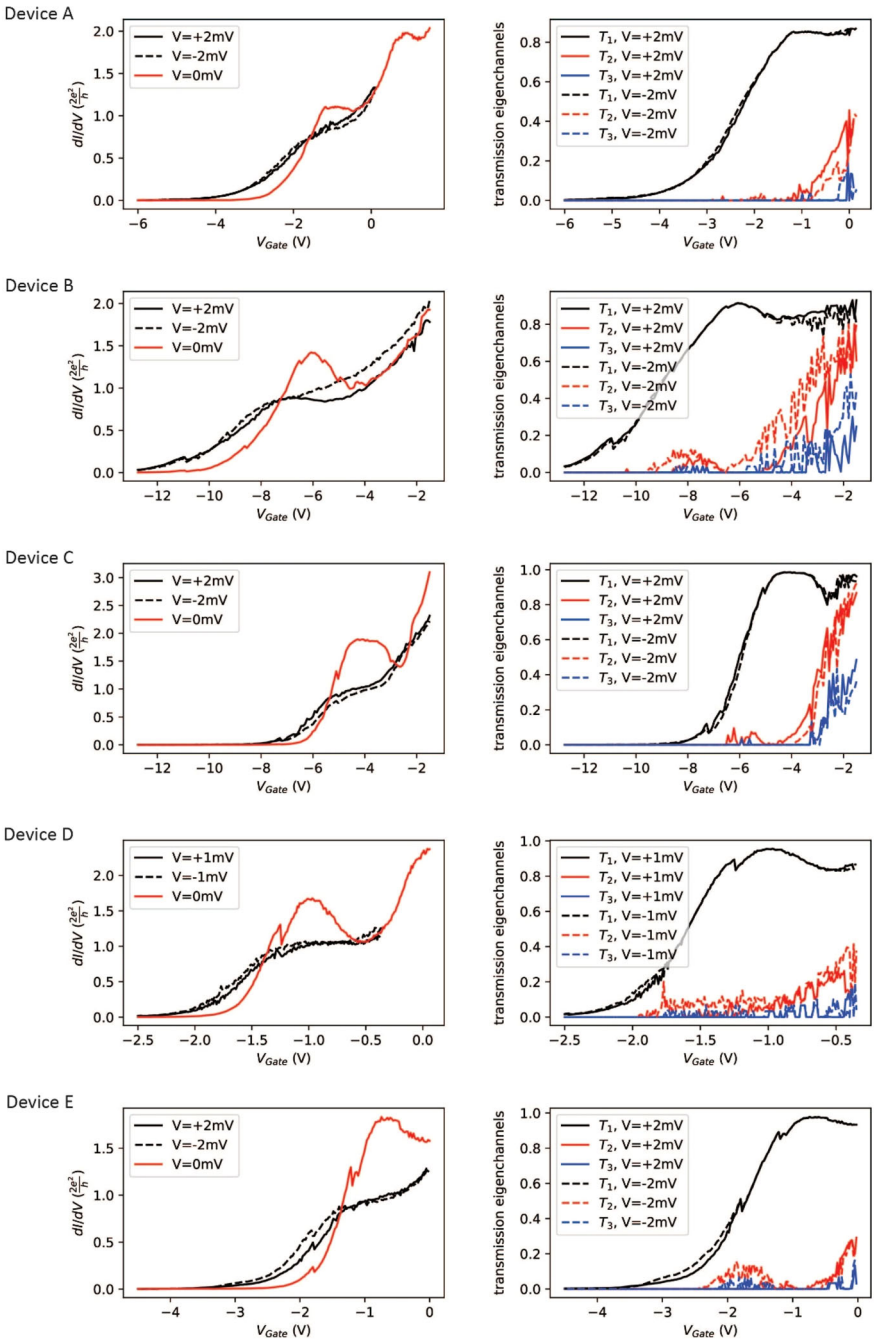


New S. Figure 7: (Left column) Panels show the measured conductance dI/dV for all reported devices, taken at positive ($0 < \Delta^* < V$), negative ($V < -\Delta^* < 0$), and zero ($V = 0$) bias voltage V. $\Delta^*$ denotes the induced superconducting gap which is 0.9 mV for device A, 0.8 mV for device B, 0.6 mV for device C, 0.52 mV for device D, and 0.85 mV for device E (see S. Figure 1). For sufficiently large bias voltage $\Delta^* < |V|$, dI/dV is the above-gap conductance. At zero bias $V = 0$, dI/dV is the enhanced subgap conductance. (Right column) Panels show the extracted transmission eigenvalues of the first three subbands contributing to the transport. All devices show QPC-like behaviour with a 1st-subband transmission rising towards one before higher subbands contribute significantly. Note that this is observed for both bias polarities.

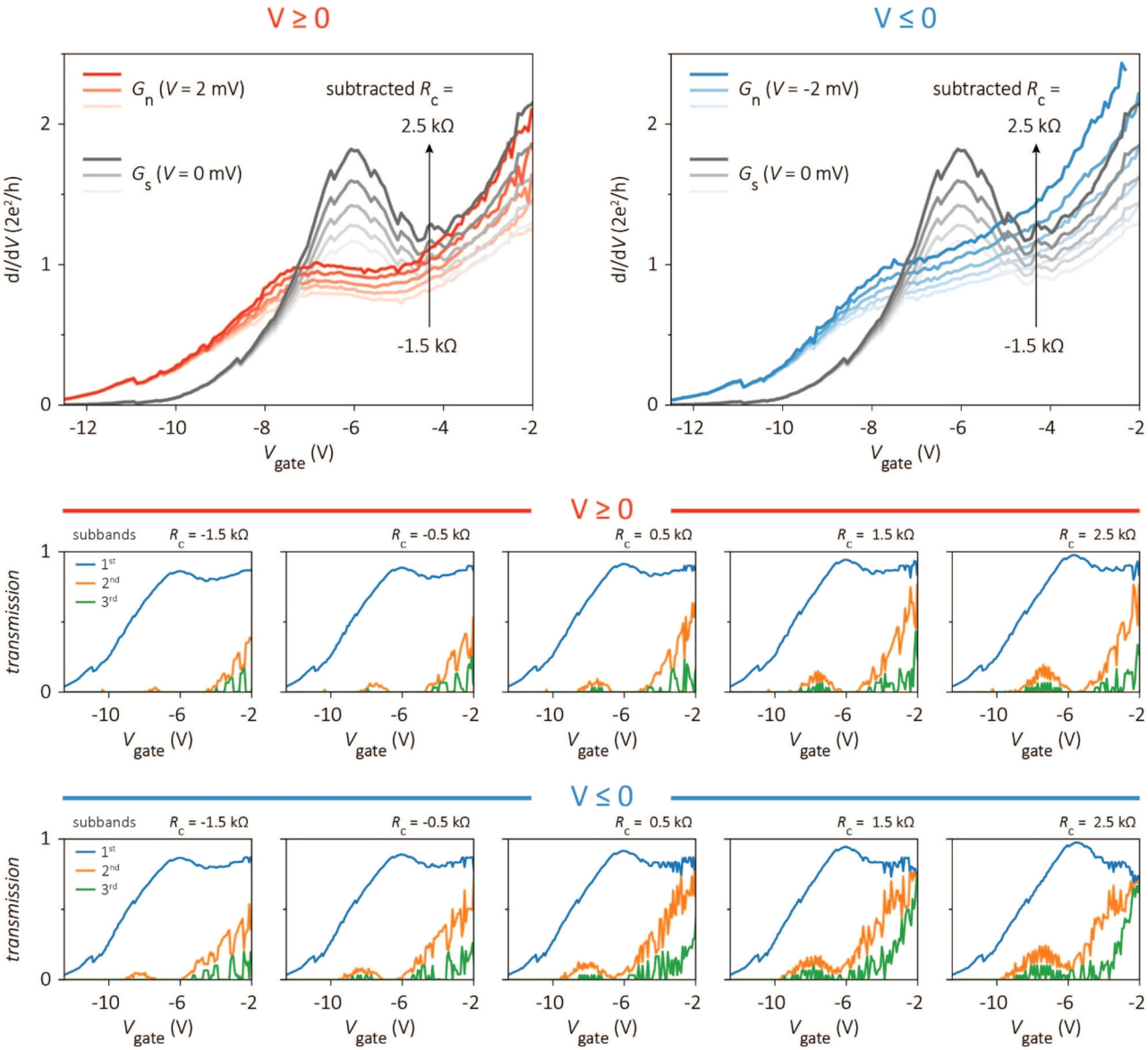


New S. Figure 8: Top row shows the measured conductance dI/dV for device B (shown in main text Figure 2a-d), taken at positive ($0 < \Delta^* < V$), negative ($V < -\Delta^* < 0$) and zero ($V = 0$) bias voltage V. $\Delta^*$ denotes the induced superconducting gap. ($\Delta^* = 0.6$ meV for device B, see S. Figure 1 caption for the other devices.) For sufficiently large bias voltage $\Delta^* < |V|$, dI/dV is the above-gap conductance Gn. At zero bias V = 0, dI/dV is the enhanced subgap conductance Gs. We have plotted Gn (for both V > 0 and V < 0) and Gs for several values of the subtracted normal metal contact resistance Rc = 2.5, 1.5, 0.5, −0.5, −1.5 kΩ. (The conductance in the rest of the publication is plotted by subtracting Rc = 0.5 kΩ which is a conservative estimation—see 'Methods'.) Negative values of Rc are not physical but considered nevertheless to test the experimental methods and the interpretation of the results. Plotted Gs and Gn increase with increasing Rc. Middle row ($V \geq 0$) and bottom row ($V \leq 0$) show the extracted transmission eigenvalues of the first three subbands (T1, T2, T3) contributing to the transport based on the conductance measured for positive (V = 2 mV) and negative (V = −2mV) bias for different values of Rc. Panels show that QPC behaviour (T1 close to 1, while T2, T3 < < 1) is independent of the excluded contact resistance value. Our extended analysis[1] finds equivalent behaviour for the other published devices (device A, C, D and E).

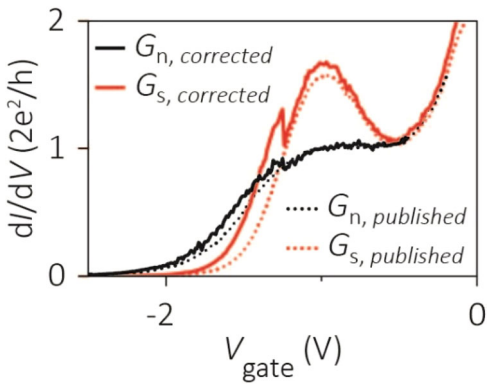


Corrected Figure 3c: Above-gap ($G_n$, black) and subgap ($G_s$, red) conductance for device D.

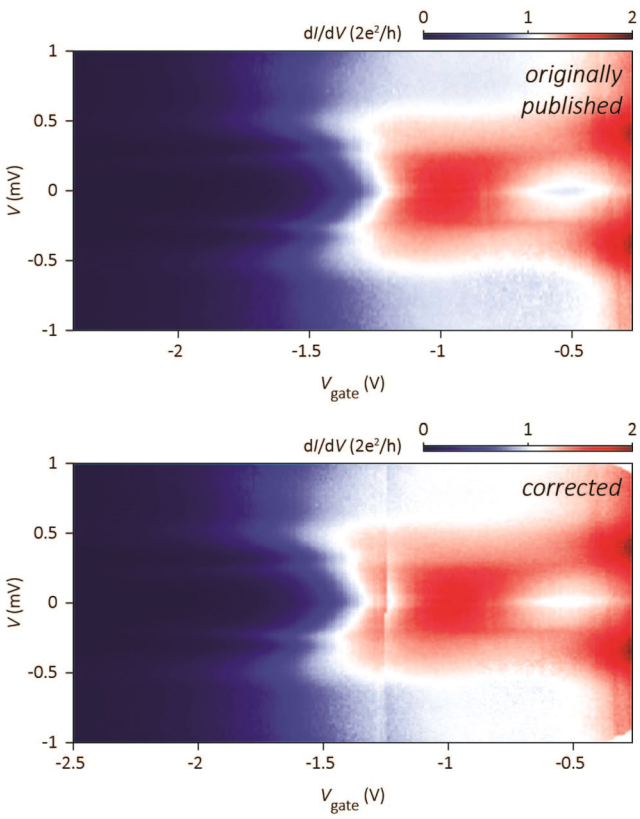


Corrected S. Figure 1i: Differential conductance dI/dV of device D in colour scale as a function of bias (V) and gate voltage (Vgate) at zero magnetic field.

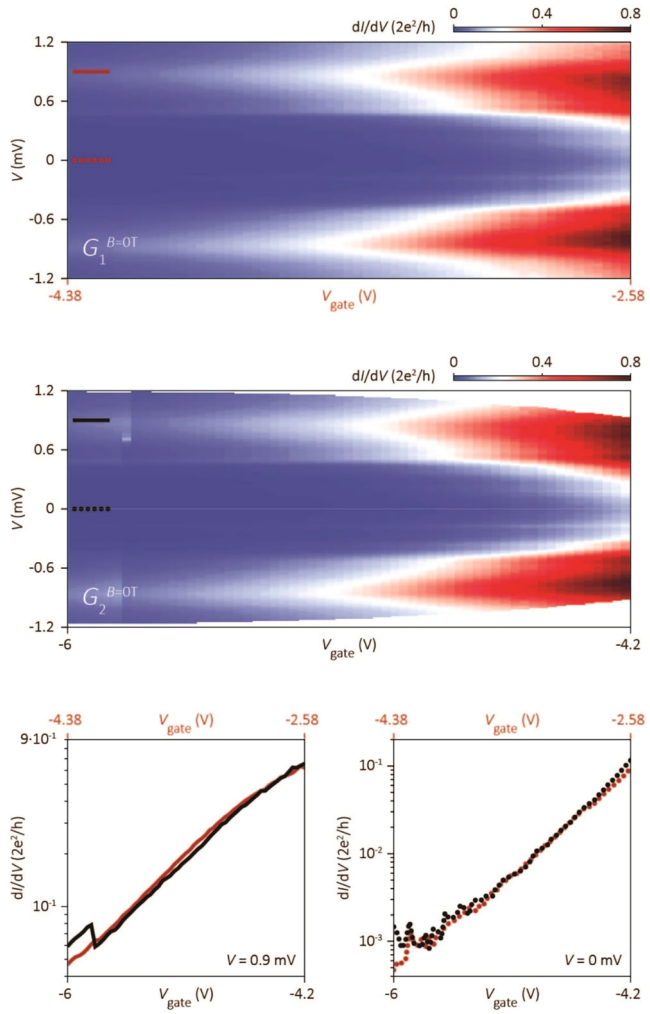


New S. Figure 9: Top row shows $G_1^{B=0T}$, the measurement from which the values of $G_n$ in Figure 4d (inset) are extracted. Middle row shows $G_2^{B=0T}$ from which $G_s$ (B = 0 T) in Figure 4d (inset) is extracted. dI/dV is the conductance, V is the bias voltage, $V_{gate}$ is the gate voltage. Note the different $V_{gate}$ values (horizontal axis) for the two panels. Bottom row, left panel, shows the horizontal line cuts at V = 0.9 mV from $G_1^{B=0T}$ (red) and $G_2^{B=0T}$ (black). Bottom row, right panel, shows the horizontal line cuts at V = 0 mV from $G_1^{B=0T}$ (red) and $G_2^{B=0T}$ (black).

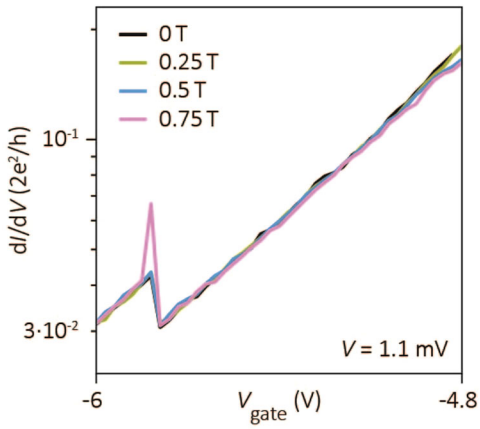


New S. Figure 10: Conductance (dI/dV) as a function of gate voltage (Vgate) taken from $G_2^{B=0T}$, $G_2^{B=0.25T}$, $G_2^{B=0.5T}$, and $G_2^{B=0.75T}$ at bias voltage V = 1.1 mV.

Figure 2d

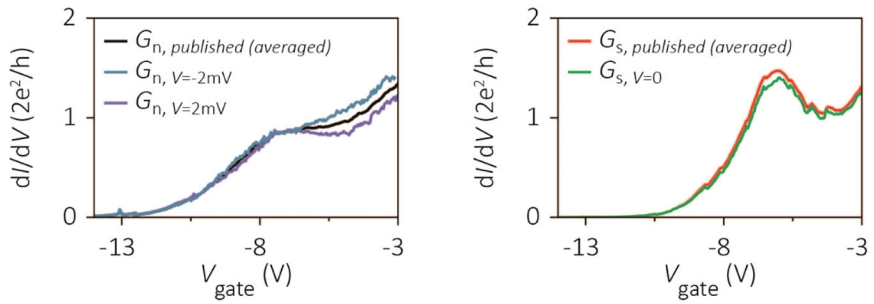


Figure 2e

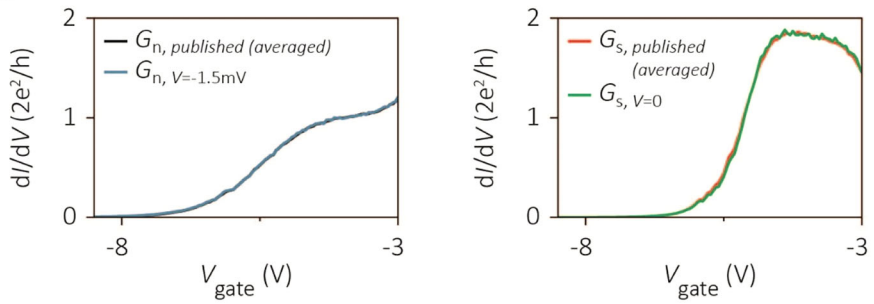


Figure 4a

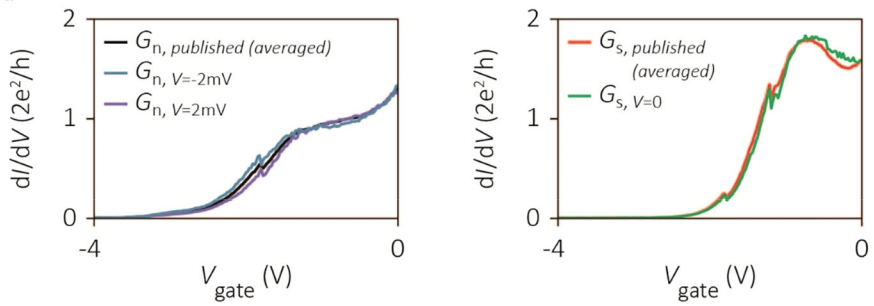


Figure 4d

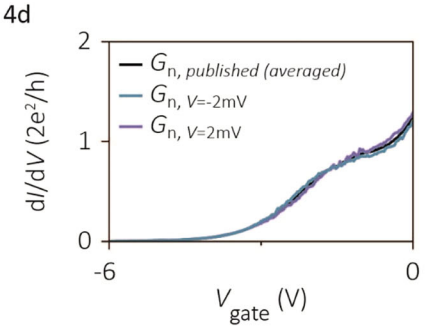


New S. Figure 11: Panels show above-gap ($G_n$) and subgap ($G_s$) conductance obtained with or without averaging over a range of bias voltage V. Originally published Figures 2d, 4a and 4d additionally include averaging over positive and negative V.

## References


1. Zhang, H. et al. Data underlying "Ballistic superconductivity in semiconductor nanowires". https://zenodo.org/record/6851435 (2022).
2. van Weperen, I. et al. Quantized conductance in an InSb nanowire. *Nano Lett.* **13**, 387 (2012).
3. Kammhuber, J. et al. Conductance quantization at zero magnetic field in InSb nanowires. *Nano Lett.* **16**, 3482 (2016).
4. Kjaergaard, M. et al. Quantized conductance doubling and hard gap in a two-dimensional semiconductor–superconductor heterostructure. *Nat. Commun.* **7**, 12841 (2016).
5. Gill, S. T. et al. Selective-area superconductor epitaxy to ballistic semiconductor nanowires. *Nano Lett.* **18**, 6121 (2018).
6. Beenakker, C. W. J. Random-matrix theory of quantum transport. *Rev. Mod. Phys.* **69**, 731 (1997).